Liquid-Phase Mass Transfer in Spray Contactors

Norman K. Yeh and Gary T. Rochelle
Dept. of Chemical Engineering, The University of Texas at Austin, Austin, TX 78712

The liquid-phase mass transfer in sprays has been measured with carbon dioxide desorption by collecting and analyzing samples of the spray. Experiments were conducted with laboratory- (0.009 to 0.13 L/s) and pilot-scale (6.4 to 12.8 L/s) centrifugal hollow-cone spray nozzles at pressure drops from 34 kPa to 138 kPa. Significant mass transfer occurred during sample collection, and a quench sampling method was developed to minimize this effect. The number of liquid-phase transfer units (N_L) due to spray impact onto walls and liquid pools was often as much as the spray N_L. Approximately 60% of the spray N_L occurs in the liquid sheet before droplet formation, and the droplet region can account for less than half of the total N_L of the spray.

Introduction

Many separations and gas cleaning applications rely on efficient mass transfer in gas–liquid contactors. Spray towers have traditionally been used as gas–liquid contactors in applications where low gas-side pressure drop is essential and a high degree of separation is not required. However, the literature for mass transfer in spray contactors is sparse compared to that for trays and packing. In particular, the liquid-phase mass-transfer characteristics of sprays have not been well described and further study is warranted.

One of the primary applications for spray contactors is in flue-gas desulfurization (FGD). The sulfur dioxide (SO_2) is removed from the flue gas of coal-fired power plants by absorbing and reacting the SO_2 with limestone slurry. Limestone scrubbing is accomplished in various types of contactors, including spray towers, venturi scrubbers, and static and mobile packed beds. However, countercurrent spray contactors are the most commonly used (Brogren and Karlsson, 1997). Several investigators (Brogren and Karlsson, 1997; DeVincentis, 1998; Gage and Rochelle, 1990) have calculated the gas-phase mass-transfer coefficient and the chemical reactions and have shown that the mass transfer is liquid phase controlled in much of the absorber.

Limited data on the N_L or $k_L a$ of spray columns have been published (Pigford and Pyle, 1951; Mehta and Sharma, 1970; Pinilla et al., 1984). Recently, Taniguchi et al. (1997) and Dimiccoli et al. (2000) attempted to model the droplet mass transfer in small-scale spray columns. Unfortunately, most of the literature focuses on laboratory-scale spray columns and small droplets (100–300 μm), compared to the 1,000–2,000 μm droplets in limestone-slurry scrubbing systems. Epstein (1975) and Jarvis and Burke (1988) reported data for pilot-scale limestone-slurry scrubbers, but interpretation of the mass-transfer data is complicated by the chemical reactions and equilibria in the limestone–SO_2 system.

Most of these studies assumed that all of the mass transfer in the column occurred in the droplet regions. However, significant mass transfer may occur in other parts of the spray contactor as well. Lin et al. (1977) and Simpson and Lynn (1977) found that the mass transfer in the sheet before/during droplet formation dominated the total mass transfer in the spray. In addition, McWhirter et al. (1995) estimated that in surface aerators, 63–66% of the overall oxygen transfer was expected to occur in the surface zone and only 34–37% in the spray zone.

Theory

Liquid exits the spray nozzle as a continuous sheet, which is expected to have high k_L and area but extremely short contact time. During the breakup process, the sheet disintegrates into ligaments and then droplets. The ligaments and droplets might be expected to have similar k_L and area, but the lifetime of the ligaments is insignificant compared to that of the droplets. Therefore, the ligaments were neglected, and only the sheet and the droplets were considered in the interpretation of the spray mass-transfer performance. The mass transfer in sprays is modeled by considering the contributions of the sheet and droplet regions separately. The N_L of each region is determined by calculating the liquid-phase mass-transfer coefficient (k_L), the interfacial area per unit liquid

Correspondence concerning this article should be addressed to G. T. Rochelle.
Current address for N. K. Yeh: ExxonMobil Upstream Research Company, Houston, TX.

volume (a_L), and the liquid contact time (t). Thus

$$N_{L,\text{spray}} = N_{Ls} + N_{Ld} = k_{Ls}a_{Ls}t_s + k_{Ld}a_{Ld}t_d \tag{1}$$

Sheet modeling

Sheet k_L. Based on the Reynolds numbers of the flows, the liquid sheets are expected to be in turbulent flow. A mass-transfer coefficient for turbulent flow can be expressed in dimensionless form as shown below (George et al., 1994)

$$\frac{k_L}{U_c} = \frac{Sh}{ReSc} \propto Re^a We^b Sc^c \tag{2}$$

According to George et al. (1994), the exponent on the Reynolds number (a) varies among the available models between $-1/2$, $-1/4$, and $1/2$. Many of the mass-transfer models do not consider the effect of surface tension ($b = 0$). However, Levich (1962) and Davies (1972) propose a Weber number dependence of $1/2$. Most absorption models predict that k_L varies with the Schmidt number to the $-1/2$ power, although an exponent of $-2/3$ has been suggested when the interface resembles a wall (Amokrane et al., 1994).

The mass-transfer coefficient of the sheet was regressed as a power law, similar in form to Eq. 2. Therefore, the mass-transfer coefficient of the sheet is assumed to be of the form

$$Sh = \frac{k_{L,s}h_o}{D} = \begin{Bmatrix} C_0\, Re_o^{C_1} We_o^{C_2} Sc^{1/2}\left(\dfrac{r}{L_b}\right)^{C_3} & \text{if } r \le L_b \\ C_0 Re_o^{C_1} We_0^{C_2} Sc^{1/2} & \text{if } r > L_b \end{Bmatrix} \tag{3}$$

Since some of the experimental data points were in the sheet, a term was also included for the position in the sheet. For the rest of the data taken in the droplet region, the contribution of the sheet k_L to the total spray N_L was included by setting the sheet length equal to L_b.

Sheet Area. In centrifugal spray nozzles, liquid exits the nozzle as a conical sheet, and as the liquid moves away from the nozzle, the cone expands and the sheet thins until it eventually breaks into droplets. The area of the sheet can be calculated, knowing the nozzle geometry and flow properties, if a few assumptions are made as in Figure 1.

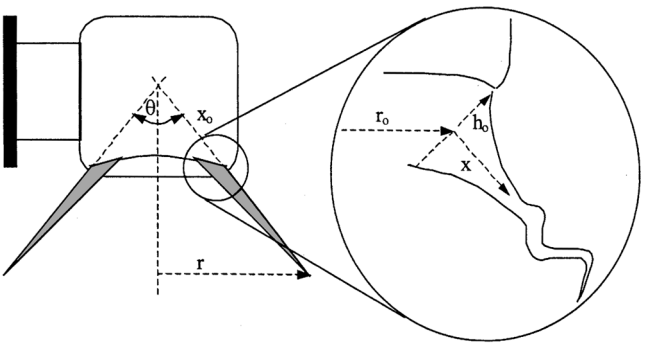

Figure 1. Calculation of sheet area.

At the nozzle exit ($x = 0$), the sheet half-thickness is

$$h_o = \frac{d_{\text{or}}}{2\cos\left(\dfrac{\theta}{2}\right)}\left(1 - \sqrt{1 - \frac{4Q_L\cos\left(\dfrac{\theta}{2}\right)}{U_o \pi d_{\text{or}}^2}}\right) \tag{4}$$

Since the sheet experiences little frictional resistance from the gas phase, the sheet velocity, U_o, is assumed constant and given by

$$U_o = \sqrt{2\Delta P/\rho_L} \tag{5}$$

The surface area of the sheet can be related to the length along the sheet surface in the x-direction. The waviness of the sheet is neglected in the following analysis. The rate of change of the sheet half-thickness (h) with distance (x) was calculated to be small ($\sim 10^{-2}$) for the nozzles used in this work. Neglecting this term allows the calculation to be linearized, and an analytical integration gives the area of the sheet. Since the volume of liquid contained in the sheet is given by the flow area multiplied by the sheet length, the area per unit volume of the sheet can be calculated

$$a_{Ls} = \frac{A_s}{\left(\dfrac{Q_L}{U_o}\right)x} = \frac{2\pi U_o}{Q_L}\left(d_{\text{or}} - 2h_o\cos\left[\frac{\theta}{2}\right] + x\sin\left[\frac{\theta}{2}\right]\right) \tag{6}$$

Sheet N_L. At the point where the sheet breaks into droplets, x is L_b. Since the sheet velocity is constant, the contact time is calculated by dividing the sheet length by the velocity. Thus, the overall k_L, a_L, and t of the sheet are determined, and the sheet N_L is given by

$$N_{Ls} = \ln\left(\frac{C_{\text{in}}}{C_b}\right) = k_{Ls}a_s\frac{L_b}{U_o} \tag{7}$$

Droplet modeling

Several models have been proposed for mass transfer in a single droplet of liquid, but most of these models were developed for liquid–liquid extraction systems. The main differences between the models are the assumed droplet hydrodynamics and mechanism of mass transfer. Small droplets can be spherical or ellipsoidal and can exhibit internal circulation. Large droplets tend to oscillate in shape, and the onset of drop oscillation is believed to result from vortex shedding from the wake of the droplet (Clift et al., 1978).

The transition between circulation and oscillation depends on several factors, most notably the presence of surfactants and the droplet Reynolds number based on continuous phase properties (Re_d). According to Clift et al., oscillation begins in pure systems when Re_d reaches values on the order of 1,000. In contaminated systems, the presence of surfactants inhibits circulation, thereby significantly increasing drag and

decreasing mass-transfer rates. Schroeder and Kintner (1965) found that spherical and ellipsoidal droplets with surfactants remain stagnant until oscillation begins at Re_d of about 200. If these oscillations are strong enough to mix the contents of the droplet, the internal resistance to mass transfer will become constant. Oscillation increases the mass transfer compared to a nonoscillating droplet.

Droplet k_L. For stagnant droplets and short contact times, penetration theory (Higbie, 1935) can be used to predict k_L from pure diffusion. The presence of circulation within the droplet increases the mass-transfer rate compared to diffusion alone. Walcek et al. (1984) found that, for small water droplets ($d < 1{,}000$ μm) falling at terminal velocity in air ($Re < 300$), the liquid-phase mass transfer can be described by the steady-state circulation model of Kronig and Brink (1950).

Mass transfer in larger droplets at terminal velocity does not agree with the steady circulation model, presumably because of turbulent circulation or oscillation at the higher terminal velocities (Altwicker and Lindhjem, 1988). Several mass-transfer models have been developed for circulating droplets (Handlos and Baron, 1957; Ruckenstein, 1967; Laddha and Degaleesan, 1978; Amokrane et al., 1994), but the predictions of the oscillation model by Angelo et al. (1966) match the experimental data most closely (Hsu and Shih, 1993). However, single-droplet experiments at terminal velocity may have limited applicability to sprays, because the spray droplet velocities may be significantly higher than their terminal velocities.

The model developed by Angelo et al. (1966) is a generalization of the penetration theory that takes into account a deforming surface. Their oscillation model assumes that the area of the droplet oscillates sinusoidally and that the contents of the droplet mix completely after each oscillation. The mass-transfer coefficient can then be calculated from the frequency and magnitude of the oscillation. A theoretical natural frequency for droplet oscillation was derived by Lamb (1945). The magnitude of the oscillation is typically difficult to measure or predict. However, at typical values of 0.3, the magnitude does not greatly impact the prediction of the Angelo oscillation model, so it can be neglected. In addition, the contact time of the droplets in the spray experiments was so short that the effects of viscous damping of oscillations could not be observed. Thus, the following semiempirical expression for the droplet N_L was used

$$k_{Ld} = C_4 k_{Ld,\text{theo}} = C_4 \left(2\sqrt{\frac{D}{\pi \tau_{\text{osc}}}} \right)$$

$$\tau_{\text{osc}} = \frac{\pi}{4}\sqrt{\frac{\rho_L d^3}{\sigma}} \tag{8}$$

The parameter C_4 was varied to match the experimental data and test how well the oscillation model described the droplet mass transfer. For experimental data with single droplets, Altwicker and Lindhjem (1988) found that the accuracy of the Angelo et al. (1966) oscillation model was improved if ϵ is set at zero and an oscillation time twice that of Lamb (1945) is used. Based on the work of Hsu and Shih (1993), the oscillation model is expected to predict droplet k_L well if C_4 in Eq. 8 is equal to 0.78 ± 0.21.

Droplet N_L. The area per unit volume of a spherical droplet is $6/d$. The droplet diameters under each set of operating conditions were obtained or interpolated from data provided by the nozzle manufacturer. Droplet coalescence and secondary breakup are neglected, so that the droplet diameter and, therefore, the area per unit volume are constant. Based on a drag calculation, the droplet velocity did not change much over the short contact time, so the velocity is assumed constant to simplify the calculation

$$N_{Ld} = k_{Ld}\left(\frac{6}{d_{32}}\right)\left(\frac{x - L_b}{U_o}\right) \tag{9}$$

Experimental Methods

Desorption of carbon dioxide (CO_2) in an air–water system was used to study the liquid-phase resistance to mass transfer. The water was buffered at a pH of 4.5 with a citric acid/sodium citrate solution. The low pH ensured that the dissolved CO_2 was not converted to bicarbonate or carbonate ion, which would not contribute to the mass-transfer driving force. Liquid samples were collected immediately upstream of the nozzle to measure the CO_2 concentration entering the spray column. Since the nozzle flow rate is a function of the pressure drop across the nozzle, the nozzle pressure was monitored and used to control the flow rate of water. The CO_2 desorbed from the spray, and then the water and any residual CO_2, was recycled.

Nozzles

The spray nozzles used in these experiments were centrifugal hollow-cone nozzles, manufactured by the Spraying Systems Company (Table 1). The nozzle designations indicate the inlet pipe size, nozzle style, material, and capacity. For example, the 1/8-A-SS-5 nozzle has a 1/8-in. pipe connection, is one of the Spraying Systems A series WhirlJet nozzles, is constructed of stainless steel, and has a capacity of 0.5 gpm (0.032 L/s) at 10-psi (69 kPa) nozzle pressure. The liquid enters the nozzle tangentially and forms a vortex in the hollow chamber of the nozzle before exiting through the orifice as a thin conical sheet. The sheet thins and disintegrates as described in the previous section to form the spray droplets.

For measurements of mass transfer during sample collection, liquid jets were, for the most part, used instead of spray nozzles. The jets had less interfacial area than the sprays and,

Table 1. Nozzle Properties

Nozzle	d_{or} (cm)	$Q/_L$ (L/s)*	$d_{V0.5}$ (μm)*	θ (°)**
1/8-A-SS-2	0.198	0.013	435	61
1/8-A-SS-5	0.318	0.032	500	67
1/4-A-SS-10	0.437	0.063	645	70
3/8-A-SS-20	0.635	0.126	910	70
3CF-SILCNB-120	5.24	9.02	1670	73

Source: Data provided by the Spraying Systems Company.
*At a nozzle pressure drop of 69 kPa.
**At a nozzle pressure drop of 138 kPa.

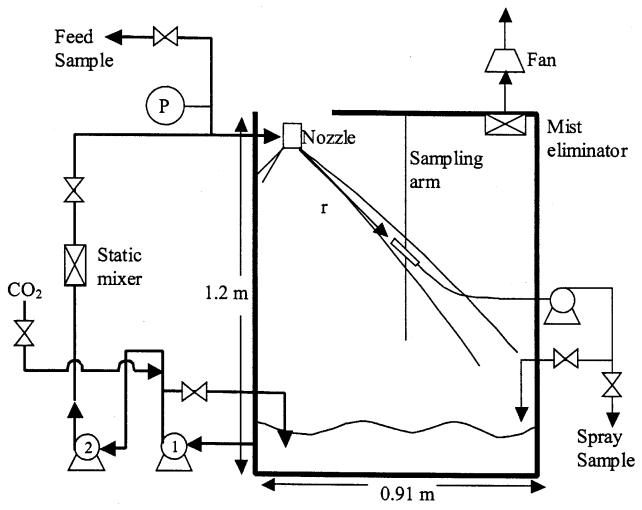

Figure 2. Laboratory spray contactor.

therefore, slower mass-transfer rates. In addition, since the jets did not thin or break up as soon as the sheets did, the simpler fluid mechanics of the jet also made extrapolating mass-transfer data to zero distance much simpler for jets than for sprays. At zero distance, the measured N_L was due to mass transfer during sample collection.

Laboratory spray contactor

The laboratory spray contactor consisted of a clear acrylic tank (0.91 × 1.2 × 0.61 m) and a sampling arm (Figure 2). Pump 1 was a 0.22-L/s diaphragm pump (ITT Jabsco model 30801-0115), which circulated water through the system and delivered the liquid to the spray nozzle.

Pure CO_2 gas was delivered via a Brooks mass flow controller and sparged into the PVC piping upstream of the nozzle. The flow rate of CO_2 was set to obtain a feed concentration of about 2 mmol/L. Pump 2 (March centrifugal pump, model MDX-3) and an in-line mixer (Koflo static in-line mixer, model 1/2-4OC-4-12-2) were used to ensure that the CO_2 was well mixed and dissolved. The second pump also increased the maximum pressure at which the spray nozzle could be operated.

The centrifugal pump was connected to the rest of the piping system by 1/2-in. PVC reinforced Tygon hose. Since the Tygon hose and the in-line mixer were clear, the dissolution of the CO_2 could be confirmed visually. In addition, the feed-sample line was translucent. If the CO_2 was not dissolving completely, then bubbles could be observed in the feed-sample line. The CO_2 solution was sprayed into the contactor, and samples of the spray were collected as a function of distance from the nozzle. The design of the spray-sample collection device is discussed later.

Pilot spray contactor

To address scale-up issues, experiments were also conducted with a commercial spray nozzle. A pilot-scale spray contactor (Figure 3) was constructed at the Separations Research Program pilot facility on the Pickle Research Campus of The University of Texas at Austin. The pilot scale system is analogous to the laboratory contactor, except that it was designed to contact only a small fraction of the total spray. This design reduced the amount of CO_2 necessary to maintain the steady-state feed concentration. In the absence of rotation in the spray, the droplets and the solute concentration were not expected to have any angular dependence. In other words, the droplet size and solute concentration were expected to vary only in the radial and axial directions. As a result, liquid sampled only in a small angle of the spray pattern should be representative of the entire spray.

The tank was constructed of polypropylene (1.9 cm thick) and consisted of two sections. Water was circulated through the system with a 15.8-L/s centrifugal pump (Ingersoll-Rand model 3×2×6 HOC), and pure CO_2 was supplied via a rotameter. The CO_2 was sparged into the feed piping approxi-

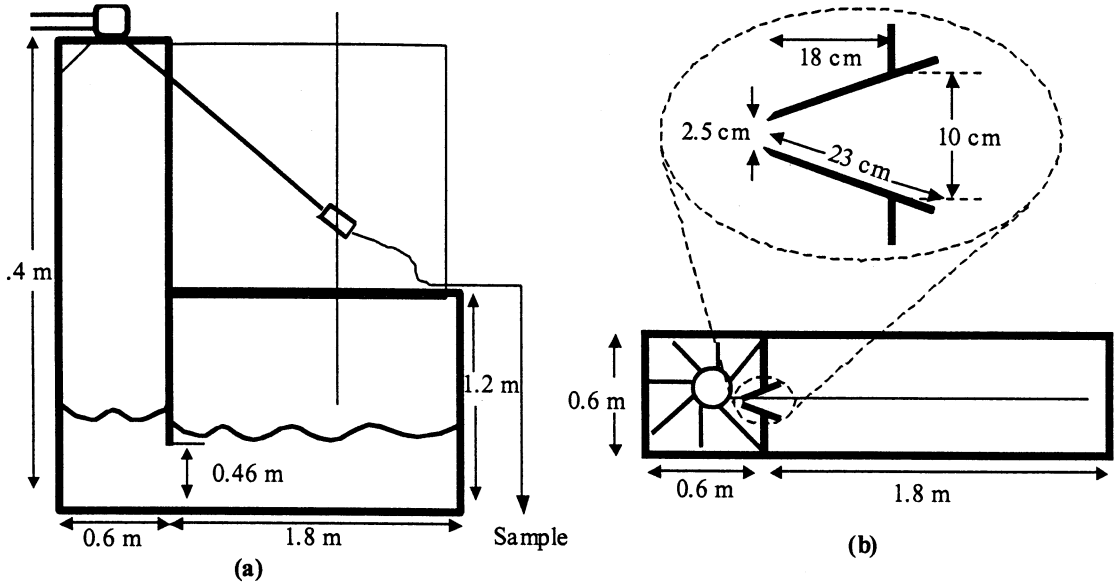

Figure 3. Pilot-scale spray contactor: (a) side view; (b) top view.

mately 15 m upstream from the nozzle to ensure that the gas bubbles would have time to dissolve. A short section of clear PVC pipe immediately before the nozzle also allowed a visual inspection of the flow.

The nozzle sprayed a solution into the first section, where most of the liquid was collected and recycled. A small ray of the spray passed between a pair of baffles into the second section of the contactor. The baffles were designed with sharp edges and angled so that the rest of the spray would be deflected and not interfere with the ray of interest. The second section of the contactor had acrylic walls to allow observation of the spray behavior and sample collection. The top of this section and the end opposite the nozzle were open to the atmosphere to allow the ambient air to circulate and remove desorbed CO_2 from the contactor. Since only a small fraction of the spray was sampled, the circulation of ambient air was sufficient to remove desorbed CO_2 from the spray tower. The spray fell into the outer section of the tank, and then the liquid was recycled.

Sample collection

Liquid samples were taken from the feed line to determine the concentration of CO_2 at the inlet to the test system. Liquid samples were collected from the spray and analyzed to obtain concentrations of CO_2. A sampling device and methods had to be developed to minimize the desorption of CO_2 from the samples during the collection event. Measurements of the mass transfer in a spray are sensitive to wall effects and the method of sample collection. Gas entrainment, secondary drop breakup, and turbulent surface renewal can result when the high-velocity spray impacts the tower walls, liquid surfaces, or the sample collection device itself.

Most of the literature for spray towers have neglected sample collection effects and assumed that all of the mass transfer is due to the spray droplets. Little or no data exist for mass transfer during spray impact or sample collection, and methods for sample collection have been crude. In single-droplet studies, more care has been taken, and methods include isolating collected droplets from the gas stream with an oil film (Amokrane et al., 1994; Kaji et al., 1985; Taniguchi et al., 1997) and collecting the droplets in NaOH solution so that dissolved CO_2 reacts before it can desorb into the gas (Altwicker and Lindhjem, 1988).

Initial samplers were designed to collect samples continuously and minimize the contact time for extra mass transfer to occur. Unfortunately, when the high-velocity spray struck the liquid surface, turbulent mixing, splashing, and frothy behavior were observed. However, if the liquid level was too low, then gas was entrained into the outlet of the sampler and into the sample line. The entrained gas and the two-phase flow in the tubing were expected to lead to too much additional desorption of CO_2. At higher sample flow rates and/or higher spray velocities, gas entrainment became even more of an issue. The mass transfer in the sample collection was measured and found to be as high as 0.8 transfer units (Yeh, 2002).

A quench sampler (Figure 4) was designed to further reduce the mass transfer during sample collection. The quench sampler consisted of an acrylic tube packed with air-filter media. Liquid was pumped out of the sampler, and the peristaltic pump was used to measure the spray flux. During sample collection, a 0.1-mol/L sodium hydroxide (NaOH) solution was also continuously fed to the top of the sampler through a 0.10-cm orifice. The orifice was drilled at a 45° angle so that the hydroxide solution was directed down into the sampler. The angle reduced the loss of hydroxide solution out the top of the sampler and facilitated mixing of the hydroxide and the liquid in the sampler.

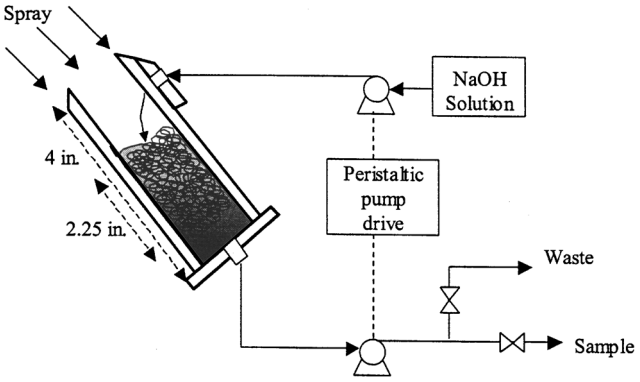

Figure 4. Quench sample collector.

The NaOH solution and the sample stream were controlled by the same peristaltic pump drive so that the ratio of NaOH solution to sample flow rate was held constant at 1.0:3.5. The NaOH solution mixed with the collected spray and reacted to convert dissolved CO_2 into bicarbonate ion, which does not desorb out of the solution. The background concentration of carbonate species in the quenching solution was measured and subtracted from the total carbonate concentration of spray samples. Typically, the total carbonate concentration of the NaOH solution was 0.3 to 0.4 mmol/L.

Results for the quench sampler are given in Figure 5, where some of the data with the overflow sampler are included for comparison. The number of liquid-film transfer units, N_L, is calculated by Eq. 7 from the measured CO_2 concentration in the inlet and sampled liquid. The average values and stan-

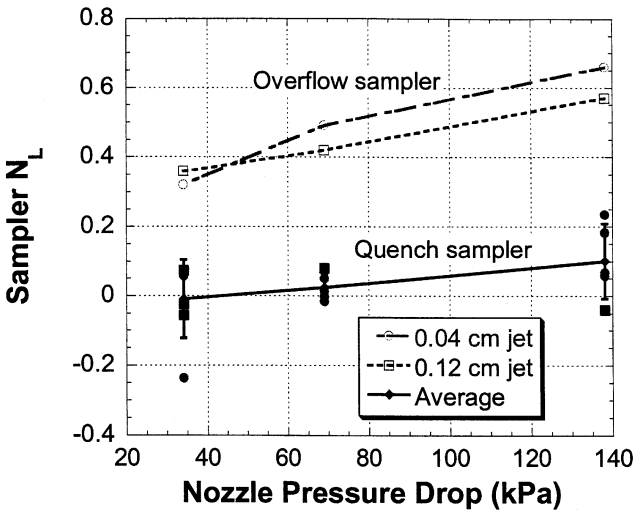

Figure 5. Mass transfer during sample collection.

dard deviations for the quench sampler N_L at each pressure are shown as well. Little or no effect of the jet diameter was observed. At nozzle pressures up to 69 kPa (velocities up to 11.7 m/s), the N_L in the quench sampler was effectively zero, compared to about 0.4 for the overflow sampler under similar conditions. At 138 kPa, data with for larger jet still showed no mass transfer in the sampler. For the smaller jet at high pressure, the mass transfer may be significant, but it is still much less than the 0.66 transfer units for the overflow sampler.

In most of the sampler characterization experiments, the jet and the sampler were oriented vertically, but during spray experiments, the sampler was pointed at the nozzle, as shown in Figure 2 and Figure 3. Therefore, experiments were also conducted with the jet and the sampler at a 45° angle to check for an effect of sampler orientation. The results agree with the earlier experiments, and provide an estimate of the uncertainty in the sampler N_L measurements. Since the effect of jet diameter was not statistically significant, average values and standard deviations were calculated for N_L at each operating pressure. A negative N_L was measured for one run at 5 psi, but it can be neglected as a statistical outlier since the standardized residual is large (Montgomery, 1997).

The N_L of the quench sampler is negligible, except perhaps at the highest velocity and lowest flow rate, where it reaches a maximum of 0.1 ± 0.1. These conditions are the same as those for the highest overflow sampler N_L. Alternatively, a more conservative conclusion would be that the quench sampler, N_L, is 0.0 ± 0.2 over the entire range of velocities and flow rates. The quench sampler N_L was assumed to be zero in the subsequent spray experiments. In any case, the quench sampler significantly reduces the mass transfer during sample collection compared to the overflow sampler. Thus, the quench system was used to measure mass transfer in all the following spray experiments, and the sampler N_L was neglected.

Sample analysis

Total inorganic carbonate was determined by an Oceanography International Model 525 Carbon Analyzer. Ten to 100 μL of the sample was injected into phosphoric acid and sparged with nitrogen to release CO_2. The CO_2 in the nitrogen was determined by infrared spectroscopy. The peak height was calibrated to give total CO_2 in the sample. Calibration solution of 1 mM CO_2 was prepared from sodium carbonate. The standard error of calibration was 1 to 2%. Replicate analyses indicated that the procedure had a reproducibility of about 1% .

Equilibrium limitations

The number of liquid-film mass-transfer units was calculated as the logarithm of the ratio of the inlet and outlet CO_2 in the liquid. Typical air contains about 350 ppm CO_2 with an equilibrium liquid concentration of 0.01 mM CO_2, which is negligible compared to the typical liquid outlet of 1 mM CO_2. The laboratory contactor was ventilated at about 100 cfm; a few specific measurements of the gas near the spray suggest that the maximum gas concentration was less than 500 ppm CO_2. The pilot-scale contactor was open on the top and ventilated by gas flow induced by the spray; no additional measurements are available to validate the assumption that CO_2 accumulation in the air was negligible.

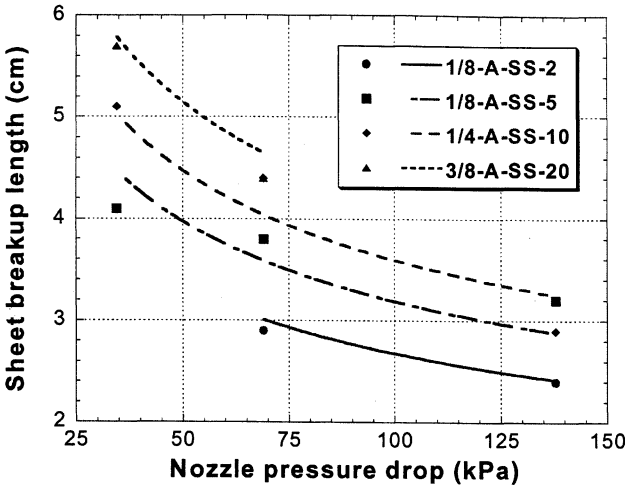

Figure 6. Sheet breakup lengths as a function of nozzle size and operating pressure (points: measurements; curves: predictions of empirical correlation Eq. 10).

Results

Using the experimental methods and quench sampling described in the previous section, the mass-transfer performance of sprays was measured directly.

Sheet breakup correlation

The sheet breakup length (L_b) was measured for each nozzle and operating pressure used in the laboratory experiments. A strobe light was used to illuminate the sheet under low ambient light so that the sheet breakup could be more easily determined. The models of Dombrowski and Hooper (1962) and Senecal et al. (1999) overpredicted the sheet breakup lengths for all of the nozzles at the operating conditions used in laboratory work. Instead, the sheet breakup lengths for the small nozzles were empirically correlated with the sheet Reynolds and Weber numbers

$$\frac{L_b}{d_{\text{or}}} = 4740 Re_i^{-0.8} We_o^{0.07} \tag{10}$$

In Figure 6, the measured and predicted sheet breakup lengths are shown for the laboratory nozzles. As the operating pressure drop is increased, the sheet lengths decrease, and the sheet lengths increase with the nozzle size.

The behavior of the sheet for the large nozzle was also observed, but the sheet breakup was difficult to measure. In flash photographs, the surface and the length of the sheet appeared irregular. Thus, sheet breakup measurements for the large nozzle were not possible. The nozzle vendor also did not have data available for the sheet lengths of the nozzles. Therefore, the prediction of the empirical correlation was used to estimate the sheet length of the pilot-scale nozzle.

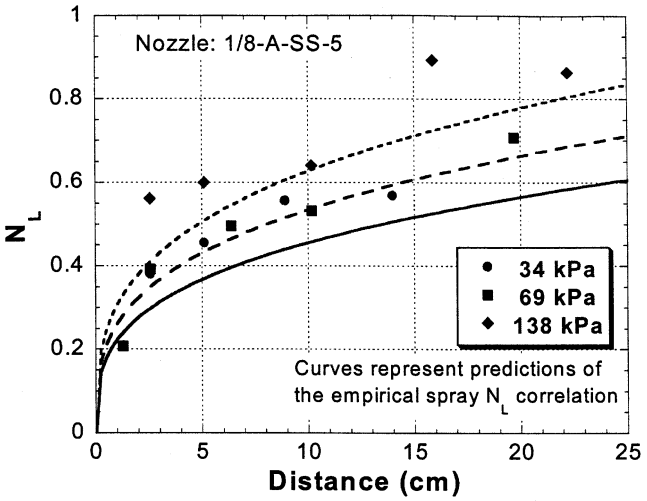

Figure 7. Spray mass transfer in laboratory experiments (nozzle: 1/8-A-SS-5).

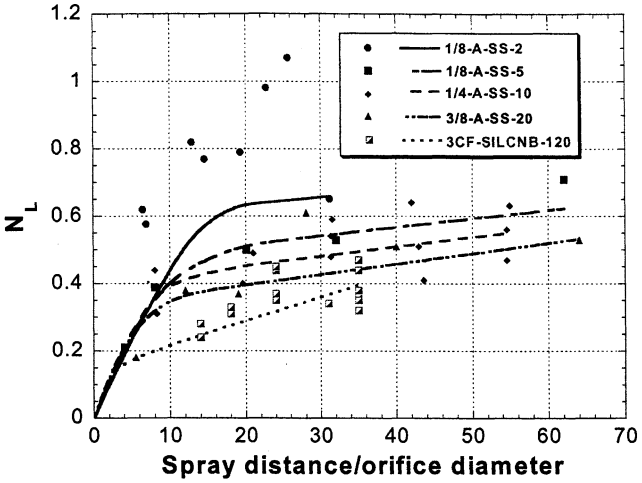

Figure 8. Effect of nozzle size on spray mass transfer ($\Delta P = 69$ kPa; curves: semiempirical model predictions).

Spray mass transfer

The N_L values for sprays were measured using quench sampling methods to eliminate spray impact and sample collection effects. The N_L data were significantly less than other reported data that did not isolate the spray from these effects. DeVincentis (1998) estimated N_L values of 1 to 3 from full-scale data for SO_2 absorption in limestone slurry. Based on these results, only 0.5 to 1.0 of the 1 to 3 transfer units that are expected in a spray may be due to the spray itself. Other sources of mass transfer must exist in a real spray contactor in order to account for the previously reported data, and they would be expected to be similar in magnitude to the spray N_L. The source of the remainder of the mass transfer is discussed later.

In the spray, N_L increased with distance, but the highest mass-transfer rates occurred near the nozzles. Figure 7 shows that the spray N_L for the 1/8-A-SS-5 nozzle was about 0.4 by the time the sheet broke into droplets (3–4 cm, depending on nozzle pressure). At a distance of 25 cm, the N_L of the spray was 0.6 to 0.8. Even before droplet formation, mass transfer in the sheet provided 50% or more of the total N_L of the spray. Mass-transfer rates in the spray droplets were much lower, and N_L increased approximately linearly with distance from the point of sheet breakup to a spray distance of 70 orifice diameters. The spray N_L exhibited a weak effect of nozzle pressure, due to the trade-off between increasing k_L and/or area and decreasing contact time.

Larger nozzles gave lower N_L at a given spray distance and nozzle pressure. In Figure 8, spray N_L data, for all of the spray nozzles are graphed vs. the distance divided by the orifice diameter of the nozzle. Even though the nozzle sizes vary by more than an order of magnitude and the flow rates cover over two orders of magnitude, the data are described well by this normalized distance. On the other hand, the data for the 1/8-A-SS-2 nozzle is noticeably different from the rest of the data. Since the 1/8-A-SS-2 is the smallest nozzle tested, it may be in a different flow regime, and the data for this nozzle were not included in the regression of the semiempirical model.

In Figure 8, the curves represent the predictions of the semi-empirical model. The parameters were regressed using the data for the 1/8-A-SS-5 through 3CF-SILCNB-120 nozzles. The sum of the squared residuals between the data and the predicted N_L values was minimized using the Solver function in Microsoft Excel. The regressed parameters are given in Table 2, with the results of a sensitivity analysis. The column labeled Sensitivity is the effect of a 10% increase in the parameter on the residual sum of squares. The columns labeled "confidence interval" are another way of expressing the sensitivity of the model to each parameter. These numbers are the change in each parameter necessary to increase the residual sum of squares by 100% .

Parameters C_1 and C_2 are the most sensitive parameters in the regression, as can be seen by the high sensitivities and narrow confidence intervals. As shown in Eq. 3, C_1 represents the Re_o dependence and C_2 the We_o dependence. The dependence of Sh on Re_o does not match any of the mass-transfer models discussed by George et al. (1994), but the value of C_1 does fall within the range covered by those models (0.5 to 1.5). The exponent on We_o is higher than expected, since only the Levich-Davies model included a Weber number dependence, and that was only 0.5.

The regression is least sensitive to parameters C_3 and C_4, which represent a variation of the sheet k_L, with distance and the correction for the droplet k_L, respectively. The un-

Table 2. Regressed Parameters and Sensitivity for Semi-empirical Model

Parameter*	Regressed Value	Sensitivity (%)	Confidence Interval (%)	
C_0	1.64×10^{-4}	25	−19.9	19.9
C_1	0.81	2745	−3.1	2.6
C_2	0.84	1578	−3.9	3.1
C_3	−0.99	1.65	−135	60
C_4	0.36	3.72	−52	52

*As defined by Eqs. 3 and 8.

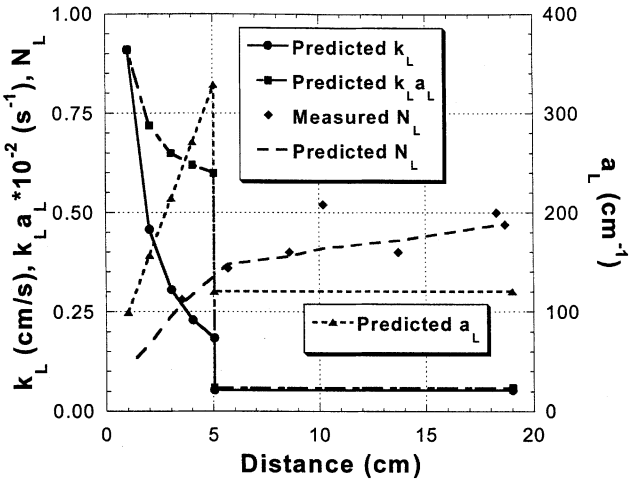

Figure 9. Comparison of k_L, area, and N_L predictions with experimental data (nozzle: 1/4-A-SS-10; $\Delta P = 34$ kPa; correlated $L_b = 5.03$ cm).

certainty in C_3 was large partly because relatively few data points were taken in the sheet. The uncertainty in C_4 was high because the slope of N_L with distance was low, and scatter in the data limited the precision with which the slope could be estimated. It is interesting to note, however, that the value of C_4 is 0.36, lower than the expected value based on single-droplet studies. Data in the literature support a semiempirical value of 0.78 $\pm$ 0.21, which lies just outside of the confidence interval estimated for C_4. Thus, the mass-transfer coefficients in the spray droplets appear to be less than they would be for single droplets.

The contributions of the mass-transfer coefficient and interfacial area to the total N_L are illustrated in Figure 9 for the 1/4-A-SS-10 nozzle at 34-kPa pressure drop. Predicted values for the area per unit liquid volume, the mass-transfer coefficient, and the product $(k_L a_L)$ are graphed as a function of distance. The resulting predictions for N_L are also compared with the experimental data. The calculated area of the sheet is a strong function of distance and increases to 330 cm^{-1} at the point of sheet breakup. To match the experimental N_L data, the regressed values for sheet k_L decrease sharply with distance.

After the sheet breaks into droplets at a distance of about 5 cm, the model assumes constant k_L and the area for the spray droplets. Since both k_L and the area of the droplets are much lower than in the sheet, the $k_L a_L$ and the slope of the N_L curve are lower as well. Although the values for k_L and the area were calculated and not verified experimentally, the predicted values for N_L are in close agreement with the experimental data points.

Mass transfer during spray impact

In a real spray tower, other opportunities for mass transfer exist besides the spray region. As a result, measurements of the mass transfer in a spray were significantly lower than expected values for the mass transfer in a spray column. The spray N_L includes mass transfer during droplet formation and droplet motion through the continuous phase. However, the spray N_L does not include interaction of the spray with other parts of a real spray contactor, for example, wall effects or interference with adjacent sprays. Previous researchers neglected mass transfer on the walls for various reasons—inability to separate spray from liquid running down the walls, area on the wall estimated to be much less than area of the droplets, to name two. However, the impact event could provide significant mass transfer by increasing k_L through turbulent surface renewal. The interfacial area at the point of impact could also be increased if droplets shatter into smaller droplets or if gas is entrained with the droplets into an accumulated liquid layer. Similar processes are used to model emissions from wastewater treatment units and sewer drop structures (Corsi and Olson, 1998).

In a real contactor, spray is expected to encounter other spray, solid surfaces, and/or liquid pools. Experiments were conducted with the 1/4-A-SS-10 nozzle to measure the significance of mass transfer during spray impact into pools of liquid. Spray was collected in a simple sampler with no packing or quench solution, and the results are shown in Figure 10. The mass-transfer data for the pool mass-transfer experiments are compared with data for the spray N_L. The solid data points were measured with the pool sampler. Therefore, these values include both the mass transfer of the spray and the mass transfer in the liquid pool of the sampler. The hollow data points represent data collected using the quench sampler.

Under all the experimental conditions, the N_L measured with the pool sampler was markedly higher than the spray N_L, measured with the quench sampler. In many cases, the N_L was twice as high as the spray N_L. The mass transfer also increased faster with distance than the spray N_L correlation does. Since the velocity of spray droplets did not change much over the short spray distances, the pool mass transfer increases as the spray flux decreases. The effect of operating pressure on the observed N_L is also more significant than it was for the spray N_L measurements. Therefore, the data also

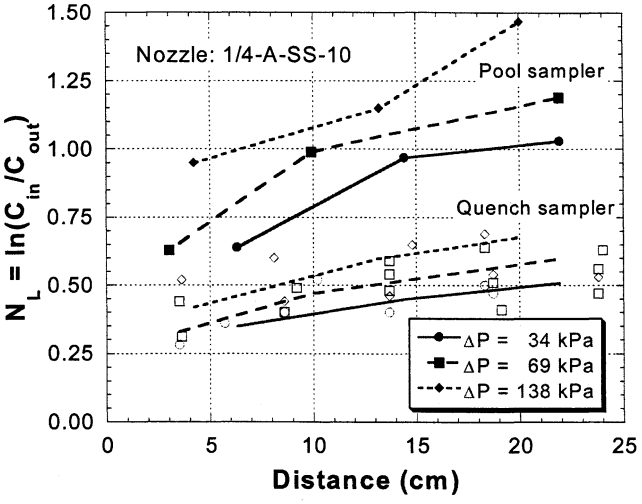

Figure 10. Comparison of pool sampler and quench sampler results (solid points: pool sampler; hollow points: quench sampler).

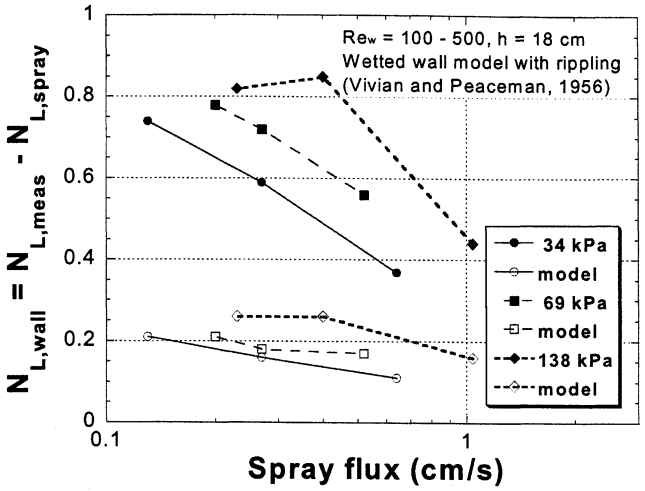

Figure 11. Comparison of wall effect with wetted-wall model.

indicate that the pool mass transfer increases with higher nozzle pressure or spray velocity.

Wall effects, or more generally, spray impact on solid surfaces, are expected to be common in spray columns, but the magnitude of mass transfer during these events is unknown. Many opportunities exist for spray to hit solid surfaces such as the column walls, spray nozzles, piping for adjacent spray headers, and other types of column internals. When spray strikes these surfaces, the droplets may shatter and generate an additional mass-transfer area. Most likely, the liquid also forms thin films on the solid surfaces, and impact events agitate the liquid film and provide higher mass-transfer coefficients.

An experiment to measure mass-transfer wall effects was designed as a model system for spray impact on solid surfaces. A flat, stainless steel plate was suspended vertically from the sample arm. The metal plate was positioned so that most of the spray hitting the plate would run down the wall instead of deflecting off the surface. The quench sampler was centered at the bottom edge of the plate to catch the liquid running down the wall without contributing additional mass transfer.

The N_L measurements in the wall-effect experiments are shown in Figure 11. The predicted spray N_L values were subtracted from the observed values to obtain the N_L due to the wall effects. The experimental values are shown in the figure as solid data points. The open data points represent N_L values predicted using the wetted wall model of Vivian and Peaceman (1956).

The experimental data have much higher N_L values than predicted using the spray N_L correlation. The mass transfer due to the presence of the "wall" ranged from 0.4 transfer units at the higher fluxes (closer to the nozzle) to 0.8 transfer units at the lower fluxes. This wall-effect mass transfer was also much greater than expected for wetted-wall mass transfer, for which the N_L was calculated to be about 0.2. The additional mass transfer is due to the spray impact on the wall.

The observed mass transfer was interpreted as the sum of the N_L due to the spray, the impact, and the wetted wall.

Table 3. Comparison of Pool and Wall Impact N_L Correlations

Coefficient*	Pool Impact	Wall Impact
ln A	-5.94 ± 1.38	-5.18 ± 1.11
B	0.72 ± 0.19	0.55 ± 0.15
C	-0.17 ± 0.04	-0.47 ± 0.07

*As defined by $N_L = AU_o^B$ (flux)^C.

The spray N_L and the wetted wall N_L were calculated and subtracted from the measured values to obtain the mass transfer during spray impact on the wall ($N_{L,imp}$). $N_{L,imp}$ was significant in the laboratory experiments, and 0.2 to 0.6 transfer units can be attributed to the spray impact. Since the spray mass transfer for the 1/4-A-SS-10 nozzle accounted for about 0.5 to 0.7 transfer units, the wall impact can nearly double the N_L of the contactor over that of the spray itself.

The effects of spray impact on the walls and into liquids were similar in magnitude. Both types of impact led to N_L values of about 0.2 to 0.7. In addition, the correlations for the impact N_L had similar dependences on velocity and flux, as shown in Table 3.

The impact of spray droplets onto solid and liquid surfaces was found to be significant and provided as much N_L as the spray region alone. Thus, a large fraction of the liquid-phase mass transfer in a real spray column is expected to occur when the spray droplets strike the walls, piping, or liquid surfaces in the contactor.

Mass transfer during spray interception of the other spray was not demonstrated to be significant in the laboratory experiments. However, the spray flux at the intersection point was lower in the laboratory experiments than it would be in a commercial spray scrubber. The higher flux in a large-scale spray column may result in more droplet collisions and additional mass transfer.

Conclusions

The mass transfer during sample collection from high-velocity gas–liquid streams can be significant. A quench sampling method was developed, which effectively eliminates mass transfer during sample collection. This new sampling method provides more accurate mass-transfer measurements so that the mass transfer in the spray and during impact on surfaces could be separated.

Most of the spray N_L occurs in the liquid sheet emanating from the spray nozzle, even before the sheet breaks into droplets. At the point of sheet breakup, the centrifugal hollow-cone nozzles provided 0.4 liquid transfer units or approximately 60% of the total N_L achieved in the spray. The high mass-transfer rates in the sheet are the result of turbulent mass transfer and high interfacial area, which compensate for the extremely short contact time of the sheet. From 10 to 60 orifice diameters, the N_L of the spray increases by only about 0.25 or 0.005 transfer units per orifice diameter. The mass-transfer rate in the droplet region was consistent with an oscillating droplet k_L, but slightly lower than the oscillation k_L model would predict.

A great deal of mass transfer occurs in spray impact and sample collection. Mass transfer during sample collection and spray impact on walls or liquid pools resulted in 0.2 to 0.8

mass-transfer units. Thus, mass transfer during spray impact was comparable to the spray N_L measured with the quench sampler. Consequently, much of the previous literature for spray columns may overestimate the spray N_L because of wall effects or sample collection issues. As much as half of the mass transfer may be occurring at the walls, at spray impact on column internals, or at the liquid surface in the bottom of the spray tower. More efficient spray-column designs can take advantage of the exceptionally high N_L per unit contactor volume for the sheet and impact phenomena by limiting the amount of contactor volume occupied by the droplets.

The nozzle pressure drop has little effect on the N_L of the spray. Higher nozzle pressures led to higher velocities in the sheet and for the spray droplets. In the sheet, k_L increased with pressure, but both the interfacial area and the contact time of the sheet decreased. In the droplet region, the higher pressure resulted in higher k_L values and area per unit liquid volume, but the higher velocities led to shorter contact times for the droplets. These trade-offs between k_L, a, and t were nearly balanced so that the overall effect of nozzle pressure on the spray N_L was only weakly positive. The major effect of increasing the nozzle pressure is the greater mass transfer during spray impact. The higher velocities caused a more violent spray impact, and more of this energy likely generated additional surface renewal and/or interfacial area.

The N_L of the spray decreases approximately with the orifice diameter as the nozzle size is increased. Spray distance was found to scale roughly with the orifice diameter over the narrow range of laboratory nozzle sizes. The pilot scale N_L data were lower, indicating that the orifice diameter had a slightly stronger effect.

The k_L values vary greatly in the different parts of the spray contactor. High k_L values were observed in the sheets emanating from the spray nozzles, and high mass-transfer rates ($k_L a$) were observed for spray impact on liquid pools and solid surfaces. However, the mass-transfer coefficients for the droplets were significantly lower. Because the k_L values varied widely, the relative mass-transfer resistances of the gas and liquid phases are also expected to vary. Unlike the CO_2–air–water system, mass transfer in the SO_2–air–water system tends to have significant resistances in both the gas and liquid phases. The mass transfer may become gas-film-controlled when the k_L is high (in the sheets or at spray impact), and then liquid-film-controlled in the spray droplets. A single value for the k_L/k_g ratio may not be sufficient to describe these systems, so the modeling and/or design of spray contactors should include a distribution of k_L/k_g ratios.

Acknowledgments

Financial support for this research was received from the U.S. EPA STAR Fellowship Program, the Chevron Corporation Endowed Graduate Fellowship in the UT College of Engineering, and the UT Graduate School via the David, Jr., Graduate Fellowship. ABB and Alstom Power provided support and insight, particularly during the early development of this research program. Dr. A. Frank Seibert of the UT Separations Research Program provided valuable feedback and assistance. Some of the spray nozzles used in this study were graciously provided by Spraying Systems Company.

Notation

a_L = area per unit liquid volume, m^2/m^3
A_s = total area of sheet, m^2
C = concentration, mol/m^3
C_i = regressed constant, from Eqs. 3 and 8 where $i = 0 \ldots 4$
D = diffusion coefficient, m^2/s
d = droplet diameter, m
d_{32} = Sauter area-volume mean droplet diameter, m
d_{or} = nozzle orifice diameter m
$d_{V0.5}$ = volume median droplet diameter, μm
h = half-thickness of sheet, m
k_L = liquid-phase mass-transfer coefficient, m/s
L = length, m
N_L = number of liquid-phase mass-transfer units
Q_L = liquid volumetric flow rate, m^3/s
r = radial position in the spray cone, as shown in Figure 1, m
Re = Reynolds number = $L_c U_c \rho/\mu$
Sc = Schmidt number = $\mu/\rho D$
Sh = Sherwood number = kL_c/D
Sh = contact time, s
t = contact time, s
U = velocity, m/s
We = Weber number = $L_c U^2 \rho/\sigma$
x = distance traveled by the spray, as shown in Figure 1, m

Greek letters

ΔP = nozzle pressure drop, kPa
θ = spray angle, °
μ = viscosity, $kg/m \cdot s^2$
ρ = density, kg/m^3
τ_{osc} = time constant (period) for droplet oscillation, s

Subscripts

c = characteristic scale
s = sheet
d = droplet
b = at sheet breakup
o = initial value at nozzle exit ($x = 0$)

Literature Cited

Altwicker, E. R., and C. E. Lindhjem, "Absorption of Gases into Drops," *AIChE J.*, **34**(2), 329 (1988).
Amokrane, H., A. Saboni, and B. Caussade, "Experimental Study and Parameterization of Gas Absorption by Water Drops," *AIChE J.*, **40**(12), 1950 (1994).
Angelo, J. B., E. N. Lightfoot, and D. W. Howard, "Generalization of the Penetration Theory for Surface Stretch: Application to Forming and Oscillating Drops," *AIChE J.*, **12**(4), 751 (1966).
Brogren, C., and H. T. Karlsson, "Modeling the Absorption of SO_2 in a Spray Scrubber using the Penetration Theory," *Chem. Eng. Sci.*, **52**(18), 3085 (1997).
Clift, R., J. R. Grace, and M. E. Weber, *Bubbles Drops and Particles*, Academic Press, New York (1978).
Corsi, R. L., and D. A. Olson, "Emission Models," *Odor and VOC Control Handbook*, H. J. Rafson, ed., McGraw-Hill, New York (1998).
Davies, J. T., *Turbulence Phenomena*, Academic Press, New York (1972).
DeVincentis, J. W., "Modeling of Limestone Slurry Scrubbing in Spray Towers with Forced Oxidation," MS Thesis, The Univ. of Texas at Austin, Austin, TX (1998).
Dimiccoli, A., M. Di Serio, and E. Santacesaria, "Mass Transfer and Kinetics in Spray-Tower-Loop Absorbers and Reactors," *Ind. Eng. Chem. Res.*, **39**(11), 4082 (2000).
Dombrowski, N., and P. C. Hooper, "The Effect of Ambient Density on Drop Formation in Sprays," *Chem. Eng. Sci.*, **17**, 291 (1962).
Epstein, M., *EPA Alkali Scrubbing Test Facility: Summary of Testing Through October 1974*, U.S. Environmental Protection Agency, Washington, DC (1975).
Gage, C. L., and G. T. Rochelle, "Modeling SO_2 Removal in Slurry Scrubbing as a Function of Limestone Type and Grind," *Proc. of the 1990 SO_2 Control Symposium*, Vol. 3, Electric Power Research Institute, Palo Alto, CA, p. 143 (1990).

George, J., F. Minel, and M. Grisenti, "Physical and Hydrodynamical Parameters Controlling Gas-Liquid Mass Transfer," *Int. J. Heat Mass Transfer*, **37**(11), 1569 (1994).
Handlos, A. E., and T. Baron, "Mass and Heat Transfer from Drops in Liquid-Liquid Extraction," *AIChE J.*, **3**(1), 127 (1957).
Higbie, R., "The Rate of Absorption of a Pure Gas into a Still Liquid during Short Periods of Exposure," *Trans. AIChE*, **31**, 365 (1935).
Hsu, C. T., and S. M. Shih, "Semiempirical Equation for Liquid-Phase Mass-Transfer Coefficient for Drops," *AIChE J.*, **39**(6), 1090 (1993).
Jarvis, J. B., and J. M. Burke, *EPRI High-Sulfur Test Center: Wet FGD Sodium Carbonate Mass-Transfer Tests*, Report CS-6029, Electric Power Research Institute, Palo Alto, CA (1988).
Kaji, R., Y. Hishinuma, and H. Kuroda, "SO_2 Absorption by Water Droplets," *J. Chem. Eng. Jpn.*, **18**(2), 169 (1985).
Kronig, R., and J. C. Brink, "On the Theory of Extraction from Falling Droplets," *Appl. Sci. Res.*, **A2**, 142 (1950).
Laddha, G. S., and T. E. Degaleesan, *Transport Phenomena in Liquid Extraction*, McGraw-Hill, New York (1978).
Lamb, H., *Hydrodynamics*, Dover Publications, New York (1945).
Levich, V. G., *Physicochemical Hydrodynamics*, Prentice Hall, Englewood Cliffs, NJ (1962).
Lin, W. C., P. A. Rice, Y. S. Cheng, and A. J. Barduhn, "Vacuum Stripping of Refrigerants in Water Sprays," *AIChE J.*, **23**(4), 409 (1977).
McWhirter, J. R., J. M. Chern, and J. C. Hutter, "Oxygen Mass Transfer Fundamentals of Surface Aerators," *Ind. Eng. Chem. Res.*, **34**(8), 2644 (1995).
Mehta, K. C., and M. M. Sharma, "Mass Transfer in Spray Columns," *Br. Chem. Eng.*, **15**, 1440 (1970).
Montgomery, D. C., *Design and Analysis of Experiments*, 4th ed., Wiley, New York (1997).
Pigford, R. L., and C. Pyle, "Performance Characteristics of Spray-Type Absorption Equipment," *Ind. Eng. Chem.*, **43**(7), 1649 (1951).
Pinilla, E. A., J. M. Diaz, and J. Coca, "Mass Transfer and Axial Dispersion in a Spray Tower for Gas-Liquid Contacting," *Can. J. Chem. Eng.*, **62**, 617 (1984).
Ruckenstein, E., "Mass Transfer Between a Single Drop and a Continuous Phase," *Int. J. Heat Mass Transfer*, **10**, 1785 (1967).
Schroeder, R. R., and R. C. Kintner, "Oscillations of Drops Falling in a Liquid Field," *AIChE J.*, **11**(1), 5 (1965).
Senecal, P. K., D. P. Schmidt, I. Nouar, C. J. Rutland, R. D. Reitz, and M. L. Corradini, "Modeling High-Speed Viscous Liquid Sheet Atomization," *Int. J. Multiphase Flow*, **25**, 1073 (1999).
Simpson, S. G., and S. Lynn, "Vacuum-Spray Stripping of Sparingly Soluble Gases from Aqueous Solutions: Part I. Mass Transfer from Streams Issuing from Hydraulic Nozzles," *AIChE J.*, **23**(5), 666 (1977).
Taniguchi, I., Y. Takamura, and K. Asano, "Experimental Study of Gas Absorption with a Spray Column," *J. Chem. Eng. Jpn.*, **30**(3), 427 (1997).
Vivian, J. E., and D. W. Peaceman, "Liquid-side Resistance in Gas Absorption," *AIChE J.*, **2**(4), 437 (1956).
Walcek, C. J., H. R. Pruppacher, J. H. Topalian, and S. K. Mitra, "On the Scavenging of SO_2 by Cloud and Raindrops: II. An Experimental Study of SO_2 Absorption and Desorption for Water Drops in Air," *J. Atmos. Chem.*, **1**, 291 (1984).
Yeh, N. K., *Liquid Phase Mass Transfer in Spray Contactors*, PhD Diss., The Univ. of Texas at Austin, TX (2002).

Manuscript received May 21, 2002, revision received Feb. 14, 2003, and final revision received Apr. 21, 2003.